Photochromism of Spiropyran Nanocrystals Embedded in Sol−Gel Matrices

Sylvie Spagnoli,*,† Dominique Block,† Estelle Botzung-Appert,‡ Isabelle Colombier,† Patrice L. Baldeck,† Alain Ibanez,‡ and Anne Corval†

Laboratoire de Spectrométrie Physique, Université Joseph Fourier, CNRS, BP 87, 38402, St Martin d'Hères Cedex, France, and Laboratoire de Cristallographie, CNRS, bat. F 25 Av des martyrs BP 166, 38042 GRENOBLE CEDEX 9, France

Received: July 20, 2004; In Final Form: January 18, 2005

Spectroscopic and kinetic properties of a new photochromic medium, consisting of nanocrystals of spyropyran molecules (1,3-dihydro-1,3,3,5′,6′,pentamethyl-spiro[2H-indole-2,2′-[2H]pyrano [3,2-b]pyridinium] iodide) embedded in an organo-silicate sol−gel film, are presented and compared to microcrystals obtained by slow evaporation of a solvent. High photoconversion efficiencies for both kinds of crystals have been observed. In microcrystals, the photomerocyanine form absorbs at 570 nm with a fading rate of 5 h, in nanocrystals the photomerocyanine form absorbs at 535 nm with a fading rate of 41 h. Therefore, the crystalline structure of nanocrystals is different from the microcrystal one.

Introduction

Photochromic organic molecules have been largely studied because of their potential applications in optical devices and memories.[1] A way to obtain a thin film with a high dye concentration and that is easy to manipulate is to use the sol−gel technique. Indeed, it has been shown that organic nanocrystals can be grown in sol−gel matrixes.[2] Thus, we can obtain particles of 100−500 nm in diameter, embedded in a sol−gel film about 1-μm thick.

Moreover, it is well-known that the structure of organic compounds depends on the growth condition.[3] So, the structure obtained via a sol−gel process and the one obtained via a slow evaporation process can be different. A difference in structure can imply a difference in photochromic properties. It is therefore interesting to compare different growth strategies.

This paper will describe the influence of two different growth processes on photochromic properties of the 1,3-dihydro-1,3,3,5′,6′,pentamethyl-spiro[2H-indole-2,2′-[2H]pyrano[3,2-b]-pyridinium] iodide, abbreviated as SPI.

The SPI molecule (Scheme 1) has been synthesized and reported as being photochromic in solution and in the crystalline state as well.[4] Photochromism of spiropyrans has been extensively studied in solution and in various matrixes,[5] but very few examples of the same reaction have been reported for the crystalline phase.[4,6] The photocoloration of the spiro form under UV irradiation results from a C_{spiro}−O cleavage followed by a cis−trans isomerization leading to the photomerocyanine form (PMC).

The large molecular conformational change involved in the photoreaction can be inhibited in a restricted geometry-like crystals. Only two cationic spiropyrans are known to undergo crystalline-state photochromism under continuous irradiation: the SPI molecule selected for this study and one of its derivatives.[4] This solid-state photochromism was suggested to be related to the presence of (i) the electron-withdrawing *N*-methyl pyridinium ring, which stabilizes the colored form, and (ii) the counterion, which enhances the free volume sufficiently to allow intramolecular rearrangement.[4] Two neutral spiropyrans have been also reported to exhibit photochromism in the crystalline state, but only under intense femtosecond laser excitation.[6] This unusual behavior was discussed in terms of transient and local lattice deformations induced by an intense laser shot, which permit the molecular structural change.

SCHEME 1 : Photochromism of SPI

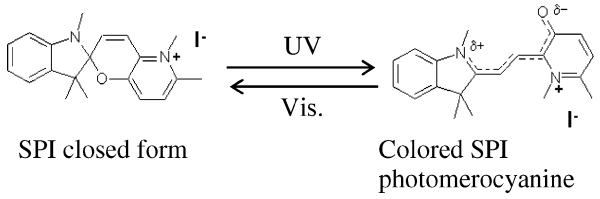

Experimental Section

Samples. The generic process used to obtain organic nanocrystals in sol−gel matrixes is described elsewhere.[2,7] This nanocrystallization results from an instantaneous nucleation followed by a controlled growth of the nuclei. The sol is synthesized under acid (HCl) catalyzed conditions by one-step hydrolysis and condensation of alkoxide precursors with 1 mol H_2O molecule per mole of alkoxide function (−OCH_3). In this study, a mixture of 50% TMOS ($Si(OCH_3)_4$) and 50% of MTMOS ($CH_3Si(OCH_3)_3$) has been used. Ethanol has been used as a solvent of the SPI molecule and to mix the water of hydrolysis with alkoxides precursors with $s = 8$, where s is the molar ratio ethanol/silicon. The organic chromophores are introduced at room temperature in the solution and are dissolved at 80 °C. The amount of organic molecules in the gel glass is expressed by the molar ratio $d =$ organic/silicon, $d = 4\ 10^{-2}$ in this study.

For the elaboration of sol−gel thin films, the viscous sol is deposited by spin-coating on a glass slide. The film thickness depends on the rotation velocity, the acceleration, and the duration of the process. With a rotation velocity of 4000rd/min

* Author to whom correspondence should be addressed. E-mail: spagnoli@spectro.ujf-grenoble.fr.
† Laboratoire de Spectrométrie Physique.
‡ Laboratoire de Cristallographie.

10.1021/jp046792r CCC: $30.25
Published on Web 04/09/2005

and an acceleration of 3000 rd/min^2, during 3 s the calibration[8] gives a thickness of 1 μm. The sizes of the so-obtained nanoparticles are determined by TEM and confocal microscopy at a wavelength of 488 nm[8] and range from 100 to 500 nm, depending on the concentration of the starting solution and on the rotation speed. The size of the nanocrystals used in this study is typically 500 nm.

The assignment of these nanoparticles to crystalline material is done in the Discussion section. They will be named nanocrystals in the following.

Microcrystals of SPI grown from ethanol by slow evaporation were also studied for comparison. Except when a unique microcrystal was used, two kinds of samples were used: (a) KBr pellets containing microcrystals and (b) evaporation of a drop of concentrated solution in ethanol, on a slide. Preparation of crystalline samples of SPI from the melt was unsuccessful because SPI exhibits thermal degradation when heated.

Bulk sol−gel matrixes containing dispersed SPI molecules with $s = 1$ and $d = 10^{-3}$, 5 10^{-4}, and 10^{-4} were prepared according to described procedures.[9] The typical thickness of the samples is about 5 mm.

TMOS is an often used silicon alkoxide precursor because of its short gelation time, but the silanol substituent of a gelled TMOS can form hydrogen bonds with the organic molecules. These interactions between molecules and the silicate network disturb the crystal formation. To minimize these interactions, MTMOS was added. The nonbridging methyl functions arising from MTMOS cover the gel pores[10] and form only van der Waals bonds with surrounding molecules.

Irradiation Conditions and Spectroscopic Measurements. All the experiments were done at room temperature.

UV irradiation on macroscopic samples was performed using a 150 W xenon lamp in association with a glass filter of 100-nm bandwidth, centered at 330 nm (with a power density of 2 mW/cm^2, during about 30 s). The corresponding absorption spectra were recorded with a Lambda-9 Perkin-Elmer spectrophotometer, either just after the end of the irradiation process, that is, typically during the first minute of the decay, or later to follow the kinetics of the thermal fading process.

Spatially resolved spectroscopic measurements on unique crystals, ranging from 500 nm to a few μm diameters, were done using a Zeiss 200 confocal microscope in which an optical fiber of 50-μm diameter joins the optical image plane of a $\times$100 objective (numerical aperture 1.3) to an Ocean Optic spectrometer. Crystals were irradiated in the UV with a 100 W mercury lamp and probed with a 100 W halogen lamp sufficiently attenuated to avoid the photoinduced back reaction. The whole spectrum is recorded in less than 2 s after the end of the irradiation process. The spectral window is [400−800 nm] and the point spread function is 250 nm. No kinetics was measured with this setup.

Results

Spectral Data. The absorption spectra resulting from the UV irradiation of three different types of solid SPI samples: a sol−gel film doped with SPI nanocrystals ($\lambda_{abs} = 535$ nm), a bulk sol−gel containing SPI dispersed molecules ($\lambda_{abs} = 550$ nm), and microcrystals embedded in a KBr pellet ($\lambda_{abs} = 570$ nm), recorded just after the end of the irradiation process, are collected in Figure 1.

The absorption spectrum of irradiated microcrystals in KBr is similar to the one obtained previously for a thin solid film,[4] whereas the maximum absorption value is shifted by about 50 nm to the blue for nanocrystals in the sol−gel matrice. To characterize unambiguously the PMC absorption spectra, spatially resolved spectroscopy using an optical microscope was conducted on unique crystals.

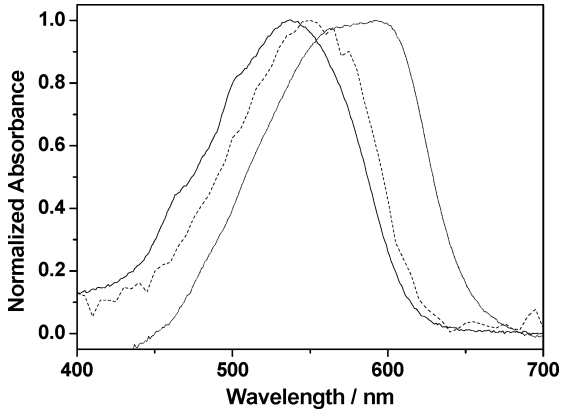

Figure 1. Normalized absorption spectra just after UV irradiation of a sol−gel film doped with SPI nanocrystals (—), a bulk sol−gel containing SPI dispersed molecules (•••), and microcrystals of SPI embedded in a KBr pellet (---).

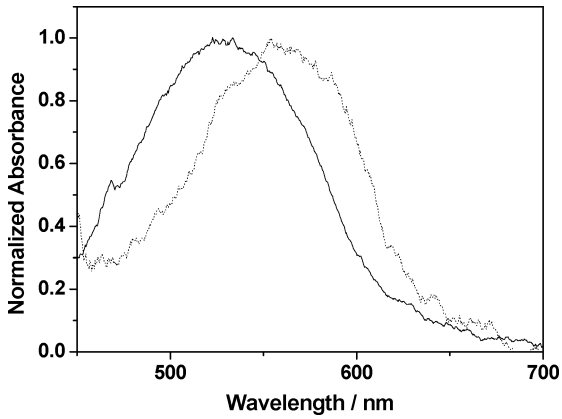

Figure 2. SPI absorption spectra obtained with the confocal microscope setup of one nanocrystal embedded in a sol−gel matrice (—) and of one microcrystal (•••), just after irradiation.

The absorption spectra of a unique nanocrystal of 500-nm diameter (embedded in the sol−gel matrice) and of a unique microcrystal of a few μm thick, recorded just at the end of the irradiation process, are shown in Figure 2. Their maximum absorption wavelengths are, respectively, 535 and 570 nm. The spectrum measured for a unique nanocrystal is identical to the one obtained for the whole film containing nanocrystals, whereas there exists a small discrepancy between the spectrum shapes of an isolated microcrystal (Figure 2) and of microcrystals in KBr (Figure 1), the second one being a little bit broader but centered at the same wavelength. This small difference could be assigned to scattering or polarization effects.

Kinetics Measurements. The thermal decay was measured over several hours in the dark. The decay curves were fitted to either mono- or biexponential decay models using Origin 6.0 for Windows. Equation $A = B \exp(-kt) + C$ or $A = B_1 \exp(-k_1 t) + B_2 \exp(-k_2 t) + C$ was chosen on the basis of χ^2 and R values. In each fit, C has to be taken different from zero. This shows that a very slow (permanent?) component is systematically induced by the irradiation.

In Irradiated Sol−Gel Films Doped with Nanocrystals. The absorption decrease at 535 nm, accompanied by a concomitant increase of the UV band of the closed form (Figure 3), can be fitted by two exponential functions (Figure 5). The corresponding fading rate constants are, respectively, $k_1 = 6.7\ 10^{-5}$ s^{-1}

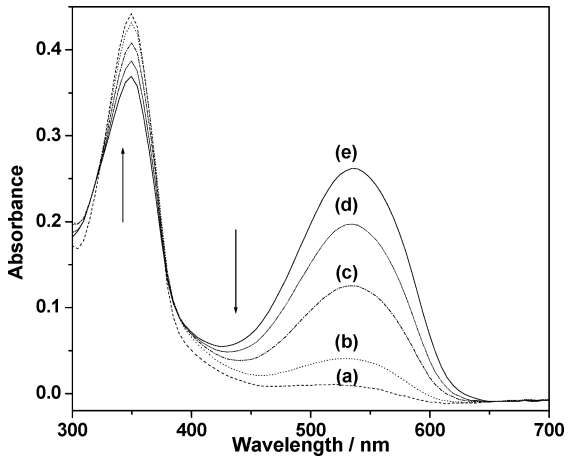

Figure 3. SPI absorption spectra obtained with the Perkin-Elmer spectrophotometer of a sol−gel film doped with nanocrystals, taken before UV irradiation (a), just after irradiation (b), 7 h after (c), 83 h after (d), and 181 h after (e).

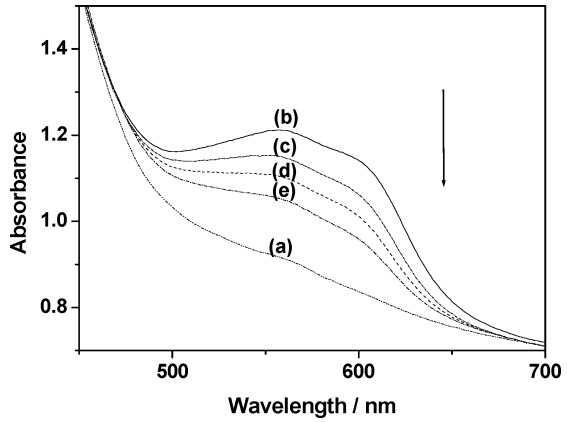

Figure 4. Absorption spectra obtained with the Perkin-Elmer spectrophotometer of SPI microcrystals embedded in a KBr pellet, taken before UV irradiation (a), just after irradiation (b), after 54 min (c), after 150 min (d), and after 320 min (e).

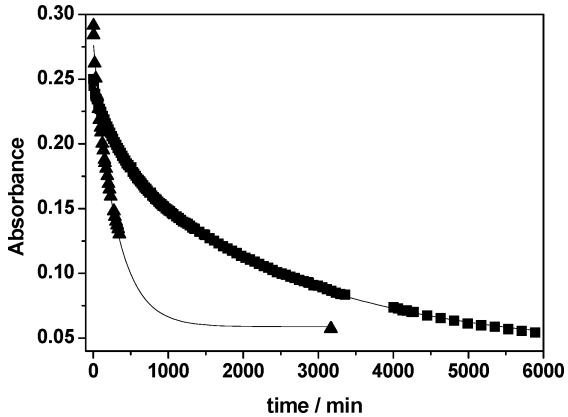

Figure 5. Thermal bleaching kinetics of PMC in nanocrystals embedded in a sol−gel film at 535-nm experimental data (■), fit (solid line). Thermal bleaching kinetics of PMC in microcrystals in a KBr pellet at 560-nm experimental data (▲), fit (solid line). The absorbance is corrected by the absorbance before irradiation for both samples.

($\tau_1 = 250$ min) and $k_2 = 6.8\ 10^{-6}\ s^{-1}$ ($\tau_2 = 2450$ min). The proportion of each component is given by the amplitude obtained with the exponential fit and amounts to 20% for the fast component and 80% for the slow one.

For Microcrystals in KBr Pellets. The fading rates are much more difficult to measure precisely, because of scattering, which

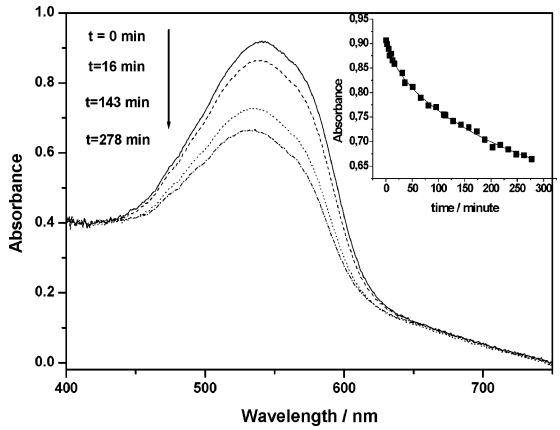

Figure 6. Absorption spectra obtained with the Perkin-Elmer spectrophotometer of SPI dispersed molecules in a sol−gel matrice just after irradiation, 16 min later, 143 min later, and 278 min later. The thermal bleaching kinetics for PMC, taken at 550 nm, is given in the insert: the absorbance before irradiation has been subtracted to the experimental data (dots) and the solid line is the biexponential fit.

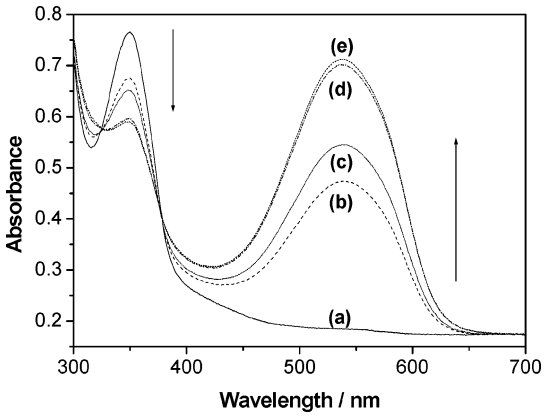

Figure 7. Absorption spectra of SPI nanocrystals in a sol−gel matrice before irradiation (a), after 3 min (b), 5 min (c), 16 min (d), and 20 min (e) of UV irradiation.

results in a flattening of the spectra (Figure 4). A decay rate $k = 5.5\ 10^{-5}\ s^{-1}$ ($\tau = 300$ min) is nevertheless easily extracted from the data at 560 nm (Figure 5).

For Dispersed Molecules in Sol−Gel Matrixes. The absorption decay at 550 nm is biexponential (insert in Figure 6), with $k_1 = 8.3\ 10^{-4}\ s^{-1}$ ($\tau_1 = 20$ min) and $k_2 = 6.7\ 10^{-5}\ s^{-1}$ ($\tau_2 = 250$ min).

Photoconversion Efficiency. An important question concerning photochromism in crystals is whether the reaction occurs in the bulk or is limited to surface and defects. It was previously proposed, from the comparison of X-ray data obtained on SPI powder before and after UV irradiation,[4] that the reaction is not limited to surfaces and induces an irreversible disorder inside crystals, but no estimate of the reaction efficiency was reported. Saturation of the absorption of the stable form generally prevents the determination of the photoconversion efficiency in crystals from optical measurements. No saturation is observed in the absorption spectra of the nanocrystals because of their small sizes, and the decrease, upon UV irradiation, of the absorption band at $\lambda_{max} = 350$ nm (Figure 7) gives a lower limit of 50% to this efficiency. A similar estimate can be given for a very thin film of crystalline SPI obtained by evaporation on a slide of a concentrated solution in ethanol (Figure 8). This high transformation efficiency indicates clearly that the reaction occurs in the bulk for the two types of crystals studied here.

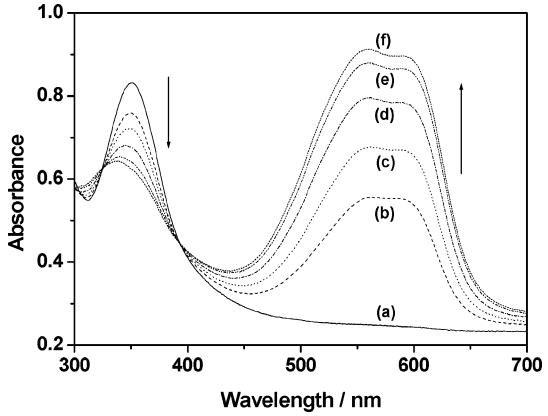

Figure 8. absorption spectra of SPI microcrystals obtained by evaporation of a concentrated solution in ethanol, before irradiation (a), after 1 min (b), 3 min (c), 7 min (d), 14 min (e), and 20 min (f) of UV irradiation.

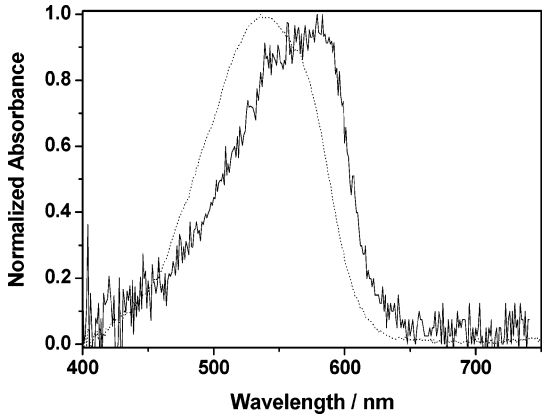

Figure 9. Normalized absorption spectra of SPI dispersed molecules in a sol−gel matrice, taken 278 min after UV irradiation (···) and the difference of two absorption curves taken just after UV irradiation and 7 min later (—).

Discussion

Kinetics and Spectral Analysis. We have shown that strong differences exist between nanocrystals embedded in sol−gel matrixes and microcrystals. Their PMC absorption spectra are different (Figure 2). These spectra thermally decrease with time in intensity, with different rates.

In thin films doped with nanocrystals, dispersed molecules could have been trapped during sample preparation and their contribution must be considered. To do that, a brief study of dispersed molecules in sol−gel is necessary.

For Dispersed Molecules in Sol−Gel Matrixes. The kinetics of the thermal fading can be fitted with two exponentials with $\tau_1 = 20$ min and $\tau_2 = 250$ min. To separate spectrally the two contributions, we have made the following subtraction between two spectra recorded at different times t after the end of irradiation. We have subtracted the absorption spectrum recorded at time $t_2 = 7$min to the one obtained at t_1 just after irradiation. As $\Delta t = t_2 - t_1 \ll \tau_2$ ($\tau_2 = 250$ min), the decay of the contribution corresponding to τ_2 is negligible on this time scale and the resulting spectrum corresponds to the fast contribution. On the other hand, an absorption spectrum taken at $t \gg \tau_1$ (20 min) reflects mainly the contribution corresponding to τ_2 (if t is too large, the spectrum corresponding to the parameter C of the fit will spoil the spectrum associated with τ_2). The so-determined spectra, given in Figure 9, are a short-lived one absorbing at 565 nm and a long-lived one absorbing at 540 nm.

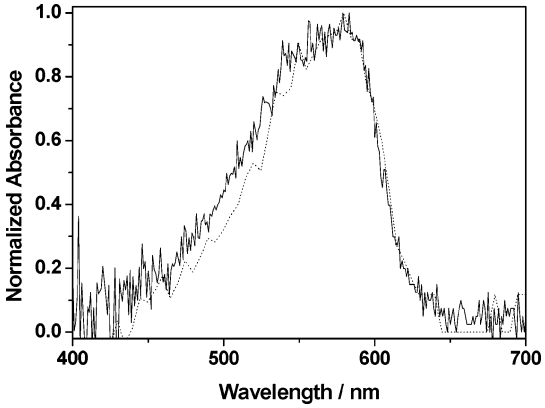

Figure 10. Normalized absorption spectrum of SPI dispersed molecules in a sol−gel matrice, corresponding to the difference between two absorption curves taken just after UV irradiation and 7 min later as in Figure 9 (—). The same for nanocrystals in a sol−gel film (---).

Moreover, we have studied the thermal fading for three samples with different concentrations $d = 10^{-4}$, $d = 5\ 10^{-4}$, and $d = 10^{-3}$; for all samples, the kinetics is the same with the same proportion between the slow and the fast component. We can therefore consider that there is no aggregation in these samples.

In Irradiated Sol−Gel Films Doped with Nanocrystals. The spectrum recorded at $t_2 = 7$min has been subtracted to the one obtained at t_1 just after UV irradiation, and the resulting spectrum (Figure 10) is very similar to the one obtained in a similar way for dispersed molecules in a sol−gel matrice (Figure 9). From this, we conclude that SPI dispersed molecules are present in the sol−gel film doped with SPI nanocrystals. Therefore, as the spectrum corresponding to the lifetime of 250 min associated with SPI dispersed molecules has a significant contribution at $\lambda = 535$ nm (see Figure 9), the observation of such a lifetime at this wavelength in a sol−gel film doped with nanocrystals (see Figure 5) is expected. We conclude that this lifetime is not related to nanocrystals and reflects only the contribution of SPI dispersed molecules.

To summarize, the merocyanine form absorbs at $\lambda_{abs} = 535$ nm with a lifetime $\tau = 2450$ min in nanocrystals and absorbs at $\lambda_{abs} = 570$ nm with a lifetime $\tau = 300$ min in microcrystals.

Structural Analysis. It is now necessary to characterize the nature of the nanoparticles embedded in the sol−gel films. Pictures obtained from confocal transmission microscopy give information about the sizes of the nanoparticles but do not demonstrate unambiguously their crystalline character. Moreover, the crystalline order cannot be checked by X-ray diffraction because the low scattering factors of the organic phase compared to those of the inorganic matrice do not permit such analysis for the doped sol−gel film. In favor of a crystalline character of these nanoparticules, we can mention that crystalline nanoparticles of different organic molecules have been previously obtained using the same preparation technique.[13]

To go further, we have visualized thin sol−gel films doped with SPI nanocrystals with an MEB Quanta 200 from FEI in low vacuum mode ($P = 1$ mbar), with an acceleration tension of 20 kV. In composition mode, the contrast is not good enough but in topographic mode it is possible to distinguish crystals through sol−gel cracks (Figure 11a−c). Moreover, during sample preparation, few crystals have grown on the surface (Figure 11 d), it is therefore possible to obtain crystals with the spin coating technique.

Growth Technique and Photochromic Properties. It should be underlined that the crystallization techniques used to prepare

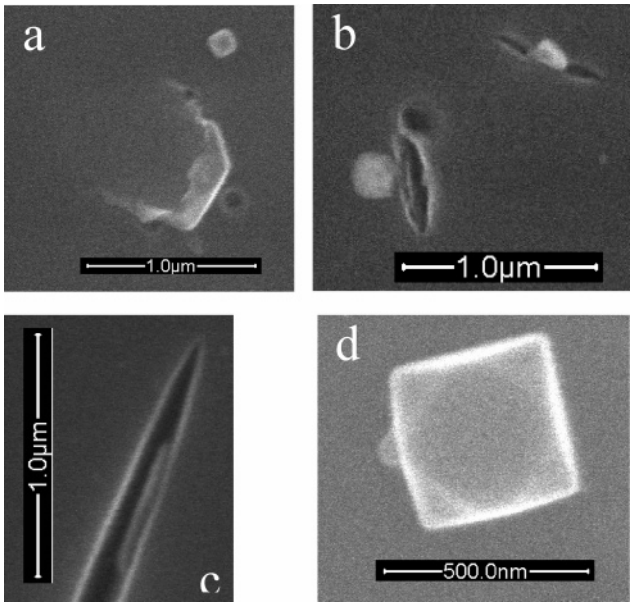

Figure 11. (a−d) MEB pictures of thin sol−gel films doped with SPI nanocrystals. The spin-coating characteristics are rotation velocity 4000 rd/min and acceleration 3000 rd/min^2, during 3 s acceleration tension 20 kV. Concentrations for pictures a and d are $d = 3\ 10^{-2}$ and for pictures b and c are $d = 4\ 10^{-2}$.

these two types of crystals are quite different, consisting of a very fast nucleation process for nanocrystals and of a slow growth during solvent evaporation for microcrystals. It has been shown that crystallization in gel can be influenced by parameters such as composition and viscosity of the gel in such a way that the crystal morphology can go from single crystal toward dendritic aggregate.[11] Less dramatic is the case of polymorphism; different crystallization techniques can imply different structures as observed, for instance, for CMONS.[12] The silicate matrice effect during the growth of nanocrystals with the same technique as the one used here for SPI nanocrystals is considered to stabilize a particular polymorph of CMONS.[13]

The irradiation of microcrystals and nanocrystals gives rise to different photochromic properties (spectra, kinetics). As we are dealing with bulk properties, we conclude that nanocrystals and microcrystals have different crystalline structures. The two crystalline structures have to be dissimilar from the point of view of intermolecular effects: steric hindrance and intermolecular interaction.

More precisely, we can think of two hypothesis, which can coexist.

First, the organization of the molecules in the nanocrystal can be such that each molecule feels a more polar environment than in a microcrystal. It has been shown that the SPI molecule,[4] as others spiropyran molecules,[14] is sensitive to the polarity of the environment: the more polar it is, the more stable is the PMC form and the more PMC absorption is blue shifted. In chloroform, SPI[4] molecules in the PMC form absorb at 587 nm with a thermal fading rate $k = 9.1\ 10^{-5}\ s^{-1}$ and in ethanol the molecules absorb at 547 nm with $k = 3.9\ 10^{-5}\ s^{-1}$.

Second, the PMC isomers can be different in the nanocrystals compared to the microcrystals. A study on another spiropyran molecule embedded in an aluminosillicate gel[15] shows two components in the PMC absorption spectrum at 475 nm and 590 nm; the first component has a fading rate 2 times smaller than the second. The first component is attributed to cis-isomers and the second one to trans-isomers.

Conclusion

The general method used to prepare nanocrystals of organic molecules in a sol−gel thin film has been successfully extended to a spiropyran compound, SPI, known to be photochromic in the crystalline phase.

The SPI nanocrystals embedded in sol−gel films show photochromic properties. However, their crystalline structure is different compared to microcrystals obtained via slow ethanol evaporation, as assessed by distinct photochromic properties (spectra, kinetics).

To proceed further, we have to know the crystalline structure of the nanocrystals. The best way to reach this goal is probably to study the polymorphism of SPI macroscopic single crystals and check, via the photochromic properties, if the nanocrystals correspond to one of these polymorphs or if the sol−gel technique gives access to a new crystallographic structure.

References and Notes

(1) (a) Crano, J. C.; Guglielmetti, R. J. *Organic photochromic and thermochromic compounds*; Plenum: New York, 1999. (b) Irie, M. *Chem. Rev.* **2000**, *100* (5), 1685−1716. (c) Kawata, S.; Kawata, Y. *Chem. Rev.* **2000**, *100* (5), 1777−1788.

(2) Ibanez, A.; Maximov, S.; Guiu, A.; Chaillout, C.; Baldeck, P. L. *Adv. Mater.* **1998**, *10*, 1540−1543.

(3) Blagden, N.; Davey, R. J. *Cryst. Growth Des.* **2003**, *3* (6), 873−885.

(4) Bénard, S.; Yu, P. *Adv. Mater.* **2000**, *12*, 48−50.

(5) For reviews on spiropyrans see (a) Bertelson, R. C. In *Photochromism*; Brown, G. H., Ed.; Wiley-Interscience: New York, 1971. (b) Ando, E.; Hibiro, J.; Hashida, T.; Moromoto, K. *Thin Solid Films* **1988**, *160*, 279−286. (c) Levy, D. *Chem. Mater.* **1997**, *9* (12), 2666−2970. (d) Schaudel, B.; Guermeur, C.; Sanchez, C.; Nakatani, K.; Delaire, J. *J. Mater. Chem.* **1997**, *7* (1), 61−65.

(6) Suzuki, M.; Asahi, T.; Masuhara, H. *Phys. Chem. Chem. Phys.* **2002**, *4*, 185−192.

(7) Sanz, N.; Gaillot, A. C.; Usson, Y.; Baldeck, P. L.; Ibanez, A. *J. Mater. Chem.* **2000**, *10* (12), 2723−2726.

(8) Botzung-Appert, E. Ph.D. Thesis, Universite Joseph Fourier, Grenoble, France, 2003.

(9) (a) Avnir, D.; Levy, D.; Reisfeld, R. *J. Phys. Chem.* **1984**, *88* (24), 5956−5959. (b) Avnir, D.; Kaufman, V. R.; Reisfeld, R. *J. Non-Cryst. Solids* **1985**, *74*, 395−406. (c) Sanchez, C.; Ribot, F. *New J. Chem.* **1994**, *18* (10), 1007−1047.

(10) Scholze, H., *J. Non-Cryst. Solids* **1985**, *73*, 669−680. Schmidt, H. *J. Non-Cryst. Solids* **1985**, *73*, 681−691

(11) Bogoyavlenskiy, V. A.; Chemova, N. *Phys. Rev. E* **2000**, *61* (2), 1629−1633.

(12) Sanz, N.; Baldeck, P. L.; Nicoud, J. F.; Le Fur, Y.; Ibanez, A. *Solid State Sci.* **2001**, *3* (8) 867−875.

(13) Brasselet, S.; Le Floc'h, V.; Treussart, F.; Roch, J. F.; Zyss, J.; Botzung-Appert, E.; Ibanez, A. *Phys. Rev. Lett.* **2004**, *92* (20), 207401(4).

(14) Wojtyk, J. T. C.; Wasey, A.; Kazmaier, P. M.; Hoz, S.; Buncel, E. *J. Phys. Chem. A* **2000**, *104*, 9046−9055.

(15) Preston, D.; Pouxviel, J.-C.; Novinson, T.; Kaska, W. C.; Dunn, B.; Zink, J. I. *J. Phys. Chem.* **1990**, *94*, 4167−4172.